Radiation and Matter: Investigating Compton Scattering

Antoni Bandachowicz

University of Chicago

May, 2022

Contents

1 Introduction

This set of experiments aims to characterize Compton scattering by analysing the relationship between the energy of the incident gamma ray (E), the energy of the scattered gamma ray (E'), and the angle at which the gamma ray scatters when interacting with the scatterer, denoted by θ. The incident gamma ray is produced from two decaying Caesium-137 sources. This report summarizes a series of experiments conducted in the spring of 2022.

2 Theory and Model Development

2.1 Derivation of the relationship between incident and scattered energy

Compton speculated that photons carry momentum. We can use this speculation to express the gamma-electron interaction in terms of momentum transfer, such that

$$p_\gamma = p_{\gamma'} + p_{e'} \tag{1}$$

where the momentum of the incident gamma (p_γ) is equal to the momentum of the scattered gamma and the scattered electron respectively. Thus, we can re-express the momentum of the scattered electron as

$$p_e = p_\gamma - p_{\gamma'}. \tag{2}$$

By introducing p_e^2 and multiplying by c^2, Compton could replace all momentum terms with hf/c. With some algebraic manipulation, we can infer the following relationship from conservation of momentum:

$$\lambda' - \lambda = \frac{h}{m_e c}(1 - cos\theta) \tag{3}$$

where λ' is the wavelength of the scattered photon and λ is the wavelength of the incident photon. By introducing $E = hc/\lambda$, equation 3 reduces to

$$E' = \frac{E}{1 + \frac{E}{m_e c^2}(1 - cos\theta)}. \tag{4}$$

Equation 4 is used in this experiment to confirm the relationship between scatter angle and scatter energy.

2.2 Dimensional Analysis of the relationship.

Equation 4 fulfills our expectations of what the relationship between E, E' and θ should be according to dimensional analysis and the conservation of energy and momentum. We see that the relationship relates three variables: E, E' and θ, with units keV, keV and degrees respectively. The variable $m_e c^2$ also has units keV, with a value of 511 keV for the electron. From conservation of energy and momentum, we would logically expect a highly energetic incident photon to give less of its momentum to the electron, and thus scatter at a smaller angle θ. Therefore, we would expect an inverse relationship between E' and θ, while also expecting a

direct relationship between E' and E. Additionally, we would want to express E' only in terms of keV, and thus we would expect a function of θ to be dimensionless (which is achieved with the cosine term). Finally, E' cannot be negative, and so we implement proportionality constants in the denominator as seen in equation 4.
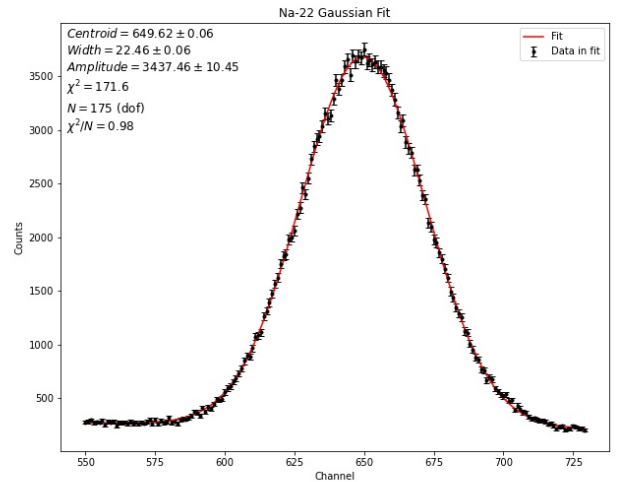
3   Calibration

Since we were using UCS-30 software paired with a PMT+NaI detector, we had to calibrate the outputted graph of the software from channel number and count, to energy (keV) and count. This will in turn give us meaningful results which will allow us to find E' for a given angle θ.

The calibration was performed by using sources of known gamma ray emission energy. A table of all 5 calibration sources is depicted below. During calibration, each source was placed right in front of the detector. The Cs-137 source located near the detector was covered with a tungsten rod, and the detector was rotated away from the Cs-137 source in order to minimize exposure to it. Note that the calibration had to be repeated since the data was gathered over the span of two days. Therefore, two linear fits are presented below.

The centroids (denoted by Ch) were found by performing Gaussian fits to the outputted channel count vs channel number spectra. For each calibration source, the spectra had to be analysed to locate the peaks caused by gamma emission.
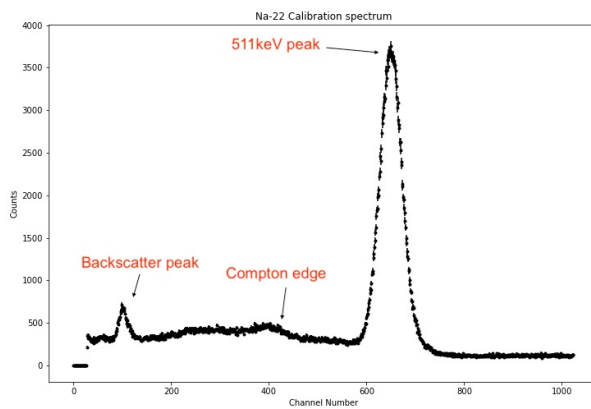
(a) Emission spectrum of Na-22. Note that the 1.27meV peak is not present due to the gain of the detector.

(b) Gaussian fit of the Na22 511keV peak.

Calibration allowed us to refine the settings to cover the expected range of E'. on the UCS-30

3

software, the fine gain was set to 2.00 and the voltage was set to 1200V. After each spectrum was analyzed and the appropriate Gaussian fits were made, the linear relationship was found for both calibration procedures. The relationship between channel number (Ch) and energy (keV) was therefore assumed to be

$$E(Ch) = A \cdot Ch + B \tag{5}$$

However, since the dominant source of error from our Gaussian fitting is channel uncertainty, we instead found the linear relationship in terms of E, where the new parameters A_1 and B_1 are related to A and B in the following manner
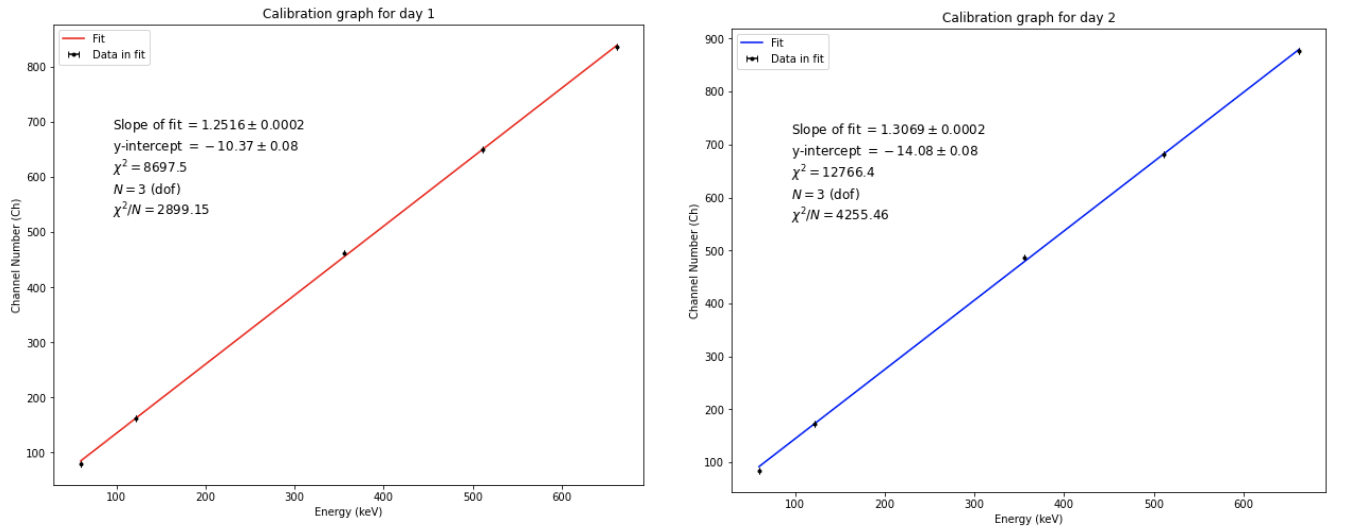
$$A_1 = 1/A \Rightarrow A = 1/A_1 \tag{6}$$

$$B_1 = -B/A \Rightarrow B = -B_1/A_1 \tag{7}$$

And the fitting function had the form: $Ch(E) = A_1 \cdot E + B_1$. The parameters A and B also had an uncertainty related to A_1 and B_1 in the following manner:

$$\delta A = \frac{A \delta A_1}{A_1} \tag{8}$$

$$\delta B = \sqrt{\left(\frac{\delta A_1}{A_1}\right)^2 + \left(\frac{\delta B_1}{B_1}\right)^2} \tag{9}$$

(a) Linear fit between channel number and peak En-
ergy for first day of data gathering.

(b) Linear fit of calibration data for the second day of
data gathering.

Figure 2: Linear Fits obtained from Calibration.

For day 1 of data gathering, we found the relationship between Energy and channel number

4

to be the following:

$$A = 1/A_1 = 1/1.25 = 0.7990 \qquad (10)$$

$$B = -B_1/A_1 = 10.37/1.25 = 8.285. \qquad (11)$$

Using the uncertainty equations 8 and 9, we find that the linear relationship for day 1 was:

$$E(Ch) = (0.7990 \pm 0.0002) \cdot Ch - (8.285 \pm 0.008) \qquad (12)$$

For day 2, the relationship between energy and channel number was calculated in the same manner as in day 1, and had the form

$$E(Ch) = (0.7652 \pm 0.0001) \cdot Ch - (10.774 \pm 0.006) \qquad (13)$$

The fits have very large χ^2 values of 8697.5 and 12766.4 for day 1 and day 2, respectively. This is in contrast with the actual fits, which seem to be fitted well to the data. This suggests that the uncertainty in the data (error variance) is largely underestimated, which in turn suggests that the uncertainties in the centroids are underestimated. We are unsure as to what could be contributing the the uncertainty of the centroids, but perhaps it is systematic error associated with the detector.

Source	Energy (keV)	Centroid (ch)	Uncertainty in Centroid (std error)
Na22	511	649.62	0.06
Co57	122	163.29	0.08
Ba 133	356	462.63	0.09
Cs137	662	836.19	0.09
Am 241	59.54	79.72	0.11

Table 1: Table showing Centroid data obtained from calibration on the first day, with uncertainty.

Source	Energy (keV)	Centroid (ch)	Uncertainty In centroid (std error)
Na22	511	680.96	0.07
Co57	122	171.91	0.09
Ba 133	356	485.40	0.07
Cs 137	662	875.66	0.09
Am 241	59.54	84.01	0.14

Table 2: Centroid data obtained from calibration on the second day, with uncertainty.

The uncertainties in the centroids, and subsequently the values for the error bars in the linear fits, were found by finding the standard error of the centroid, meaning $\delta centroid = \sigma/\sqrt{N}$ where

N is the total number of counts in the fitting sample. All angle values have an uncertainty of 0.5 degrees. All Gaussian fits had reasonable reduced-χ^2 values below 2.0.

4   Peak Shifting

The calibration for two separate days clearly showed potential sources of error. Firstly, for each day we had to wait around 30 minutes for the PMT+NaI detector to warm-up, meaning we had to wait until the outputted peaks no longer experienced shifting along the channel number axis. However, even after waiting for longer periods of time, the peaks would still shift by several counts to the right. The consequences of this is further discussed in section V.

5   Procedure for data extraction and uncertainties.

According to equation 4, changes in the scatter energy (E') are greatest for angles around 38 degrees. As such, a large quantity of the angles we decided to analyse were around the region of 38 degrees. We also decided to take measurements at the extrema (0 and 80 degrees) in order to fully capture the nature of the relationship in this angle range.

The scatter Energy (E') of the gamma rays incident from the two Cs-137 sources was measured for 9 angles. For all of the angles (except for 60 and 80 degrees), a background spectrum was first captured. This was done for us to be able to subtract counts caused by gamma rays which have not scattered from the main spectra. The spectra were first subtracted, and then the fitting was performed. For 60 and 80 degrees, a background spectrum was not captured since the vast majority of gammas incident on the detector were scattered, and our time in the lab was limited. The E' values were found by first finding the centroids of the peaks found in the subtracted PHA spectra. For angles investigated on day 1, the centroids were then inputted into equation 5, while values found on day 2 were inputted into equation 13. Table 3 shows the scatter energy values for each angle.

The uncertainty for E' was found using the equation shown in figure 3 :

$$\sqrt{(y \cdot \delta x)^2 + (x \cdot \delta y)^2 + (1 \cdot \delta z)^2}$$

Figure 3: Equation used to find uncertainty in E'.

In figure 3, x and δx are centroid values, y and δy are slope values from the linear fits (A),

and δz is the uncertainty in the intercept of the linear fit (B) obtained from calibration. The uncertainty for all angles was ± 0.5 degrees.

6 Analysis of the observed relationship between E' and θ

Angle (°)	Scatter Energy (keV)	uncert. Energy ($\pm$keV)
DAY 1		
0	672.2	0.2
19	630.2	0.2
30	580.8	0.2
40	520.5	0.1
55	438.7	0.1
DAY 2		
25	620.4	0.1
35	559.2	0.1
60	418.6	0.1
80	339.5	0.6

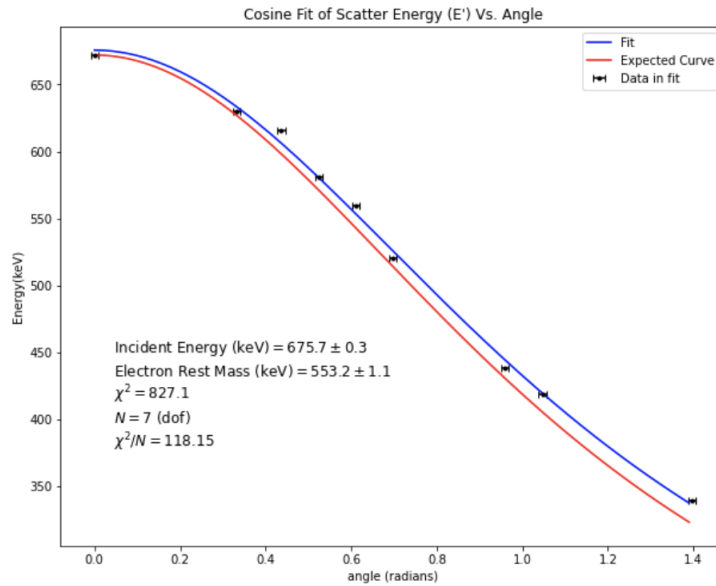Table 3: Values of scattered energy (E') for each angle, with uncertainty.

Figure 4: Fit of E' vs. θ using the equation predicted by theory.

The values shown in table 3 were plotted in figure 4, with a fitted function of the form in equation 4 overlaid over the points. This fitting gave us an observed incident energy (E) of

675.7 ± 0.3 keV and an electron rest mass of 553 ± 1 keV. Neither of the these value ranges cover the predicted values of 662keV for E and 511keV for the electron rest mass.

6.1   Goodness-of-fit And Sources Of Error

Additionally, The goodness-of-fit is characterized by our χ^2 value of 827 and a reduced χ^2 of 118.15, suggesting that our uncertainties were underestimated. The dominant uncertainty in the fitting was the uncertainty in angle. It is likely that additional error was introduced by the slider on which the detector was located. We noticed that it was difficult to position the slider optimally, perhaps because the platform on which the experiment was located was not level with the ground.

Analysing Figure 4, by comparing with the expected curve (red) following Equation 4, we see that the relationship between E and the angle does follow the predicted relationship. However, there is a shift in the data, caused by a systematic error, likely caused by the slider, as mentioned above. We also see that the curves diverge at higher angles. One possible explanation could be the fact that we did not subtract the background from points at 60° (1 rad) and 80° (1.4 rad). We assumed that at higher angles we no longer needed to subtract the background, however Figure 7 shows that this is a false assumption, since non-scattered gammas are still incident on the detector at these angles. This would artificially increase the energy values of the data, causing the two curves to diverge.

Nevertheless, the residual graph demonstrated in Figure 5 shows randomly distributed residuals, equally spaced on either side of the zeroth line, with similar magnitude in distance (from zero). This suggests that the expected cosine relationship is a good fit to the data.

Regarding individual points in Figure 4, the third data point from the left could be considered as an outlier. This is because its residual is furthest from the zeroth line. One possible explanation for this is the fact that this data point was the first point to be gathered on the second day of testing, after calibration was performed. Thus, it is likely that this point suffered from peak shifting caused by the warming-up of the detector. This shifting happened on both days, though on the first day we waited a significant period for the detector to stabilize. This shifting is also the reason for the differences in calibration relationships seen in figures 2a and 2b. After the third data point was taken out of fitting, the new incident energy E was found to be 673.1±0.3 keV and the electron rest mass was 555±1 keV.

Overall, the entire graph in Figure 4 seems to be shifted, since both of our estimated parameters are above the predicted values. We found the value of the shift by fitting a function of

the form

$$E' = \frac{672.2}{1 + b \cdot \frac{672.2}{511}(1 - cos\theta)} \tag{14}$$

where "b" is the shift, and 672.2 was chosen since this was the 0° energy we found experimentally. We found the value in this shift (after subtracting the third point) to be 0.916±0.001. This means that the ratio between the incident gamma energy and the electron rest mass is within 0.916±0.001 of predicted value. Figure 8 in the appendix demonstrates the fitting performed to find this ratio.
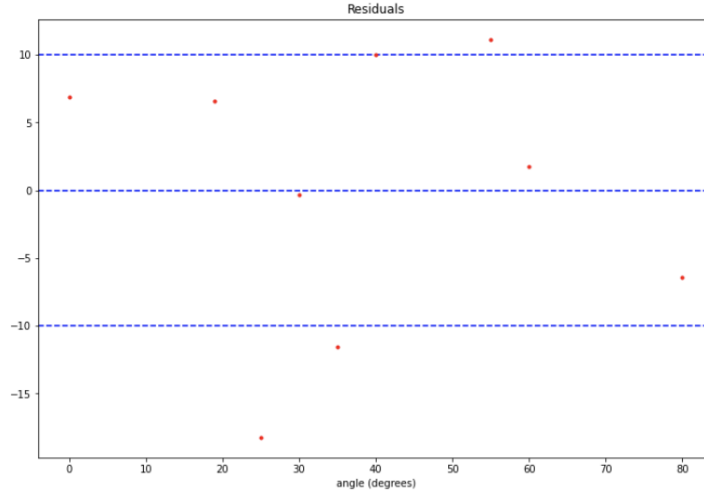

Figure 5: Residuals of the fit in Figure 4. Note the randomness in distribution, suggesting a good fit to data.
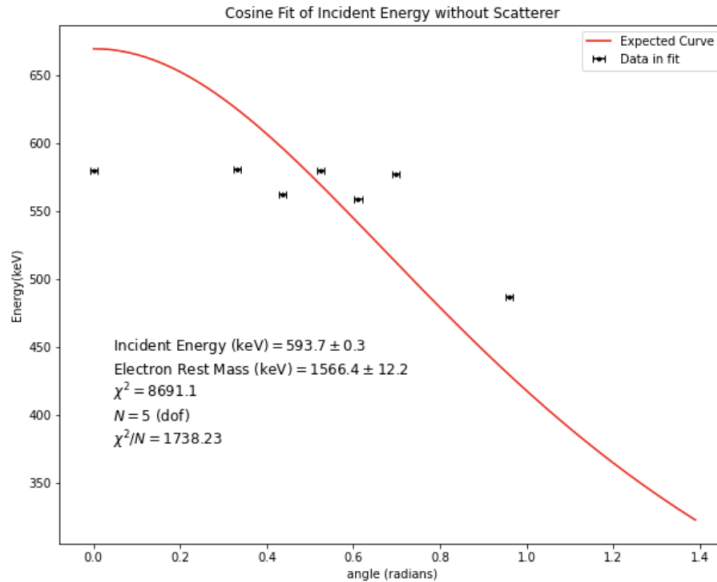

Figure 6: fit of incident energy on the detector when no scatterer was present. Notice that for angles near 60° (1 radian) the incident energy is clearly non-zero.

9

7 Conclusion

After subtracting outliers, we found that the incident energy E was 673.1±0.3 keV and the electron rest mass was 555±1 keV. High χ^2 values for all fits were due to underestimated uncertainties, which was caused by systematic error we did not consider during the experiment. The sources of error identified were a potentially slanted slider, the lack of background subtraction at higher angles, and peak shifting.

A shift was noticed in the final data, likely caused by systematic error identified above, which was quantified to be 0.916±0.001. Residual analysis of the cosine fit to data showed that predicted relationship adequately described the observed relationship between E' and θ.
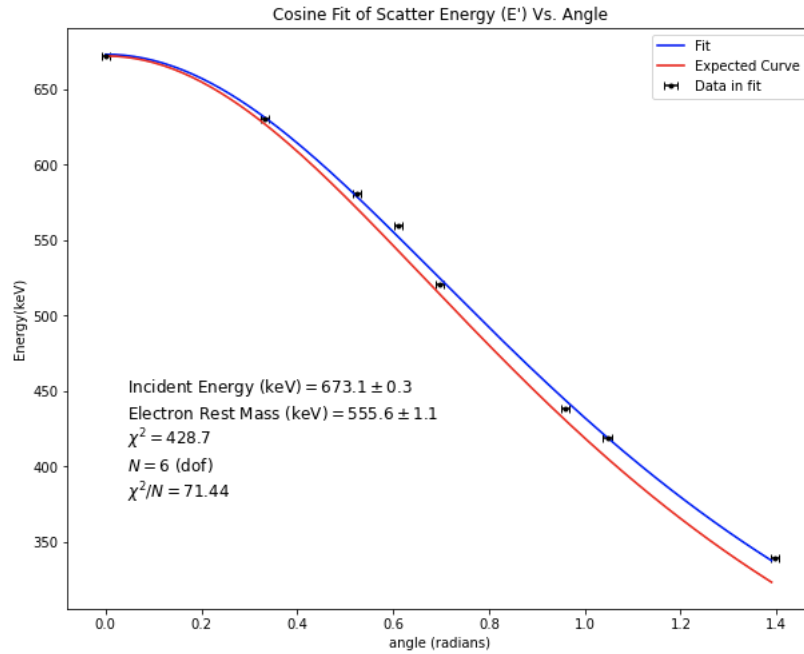
8 Appendix

Figure 7: fit of scatter energy E with the outlier point (point 3) taken out of fitting. This resulted in a lower χ^2.

Angle (°)	Incident Energy (keV)	uncertainty in Energy ($\pm$keV)
0	579.70	0.07
19	580.47	0.06
25	562.06	0.08
30	579.72	0.07
35	559.03	0.07
40	577.50	0.08
55	486.89	0.19

Table 4: Incident energy values without scatterer present, with uncertainty, calculated in the same manner as described in section V.
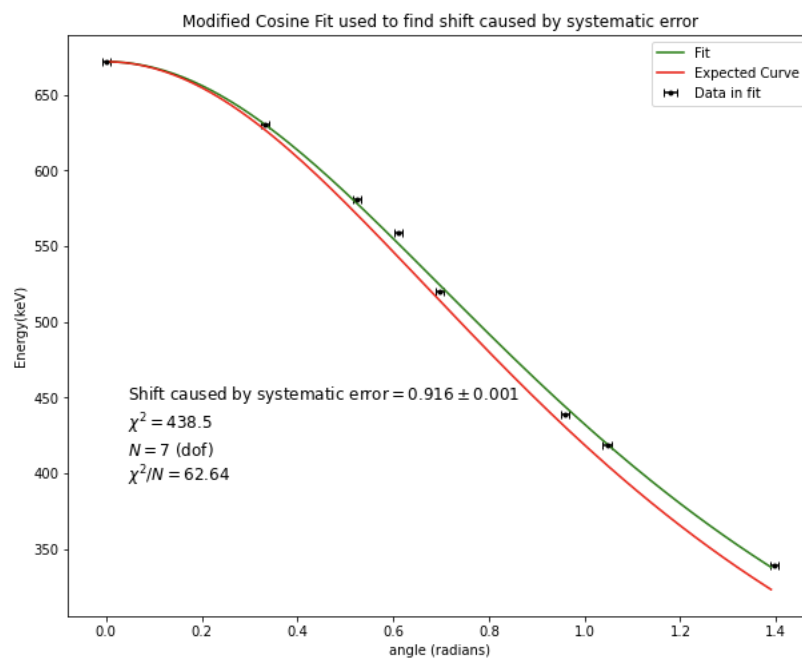

Figure 8: modified cosine fit used to find the shift in the expected relationship due to the data.